



A novel smart disinfection system using 3D-printed and electrically conductive composite hydrogel

Shaheryar A. Khan^{1,2} · Anjum Naeem Malik^{1,2} · Basak Velioglu³ · Seref Gul^{4,5} · Ibrahim Halil Kavakli^{3,6} · Ismail Lazoglu¹

Received: 21 November 2023 / Accepted: 16 January 2024
© The Author(s) 2024

Abstract

Smart materials are ushering in the era of smart and adaptable products. Hydrogels are a distinct class of smart materials that can be 3D-printed to produce smart and active structures that can be used as sensors and actuators. The development and characterization of a 3D-printable and electrically conductive composite hydrogel, as well as its application in the development of a smart disinfection system, are discussed in this article. The developed composite hydrogel has a maximum electrical conductivity of 145 S.m^{-1} , is stable up to $200 \text{ }^\circ\text{C}$, and has a 3D printable rheology. Virtuous of its electrical conductivity, the composite hydrogel was used to create a smart disinfection system. Various disinfection systems have been adopted for the disinfection of contaminated surfaces; however, most of these systems require human evacuation from the surroundings due to the hazardous nature of the virucide. The proposed system is designed to disinfect contaminated surfaces on common-use equipment and is capable of real-time activation through user interaction. It employs a thermal disinfection process at $60 \text{ }^\circ\text{C}$ for 5 min and becomes ready for the next user once its temperature drops below $55 \text{ }^\circ\text{C}$. This system consumes 1.64 Wh of energy per disinfection cycle and is suitable for scenarios with fewer than 60 user interactions in an 8-h work shift.

Keywords Smart materials · 3D printing · Capacitive sensing · Thermal disinfection systems · Disinfection on-demand

1 Introduction

Smart materials are marshaling a transformative era for various industries by enabling the creation of intelligent and adaptable products that respond predictably to external stimuli. These materials play a pivotal role in advancing

technologies and engineering applications, notably in the domain of smart sensors and actuators. They include shape memory alloys, piezoelectric materials, thermochromic materials, thermoelectric materials, and hydrogels [1, 2].

Hydrogels represent a distinct category of smart materials, characterized by their intricate three-dimensional network structure with a remarkable capacity to retain substantial amounts of water or aqueous solutions. Hydrogels are exceptionally versatile materials, boasting a wide array of applications across diverse fields, owing to their unique attributes. These applications span the domains of medicine, drug delivery systems, tissue engineering, soft robotics, and sensor technology [3].

In particular, the field of sensors has witnessed a significant surge in interest regarding hydrogels. Researchers have devised responsive hydrogel composites that incorporate other materials, such as nanoparticles or conductive particles [4, 5]. These composite materials can manifest alterations in electrical conductivity or magnetic properties in response to environmental factors, thus enabling the development of a wide spectrum of sensor types. These encompass ion,

✉ Ismail Lazoglu
ilazoglu@ku.edu.tr

¹ Manufacturing and Automation Research Center, Koc University, Istanbul, Turkey

² Present Address: National University of Sciences and Technology, Sector H-12, Islamabad, Pakistan

³ Department of Molecular Biology and Genetics, Koc University, Istanbul, Turkey

⁴ Biotechnology Division, Department of Biology, Istanbul University, Istanbul, Turkey

⁵ Present Address: Institute of Life Sciences and Biotechnology, Bezmialem Vakif University, Beykoz, Istanbul, Turkey

⁶ Department of Chemical and Biological Engineering, Koc University, Istanbul, Turkey

biological, mechanical, and touch-detection sensors, among others [1].

Hydrogels can be used in 3D printing in their hydrated or paste state. The Direct Ink Writing (DIW) technique can be used to 3D print with hydrogels opening new horizons for the development of smart and active products. 3D printing with hydrogels offers several advantages, including the ability to create smart and active products using application-specific geometries. The 3D-printed hydrogel dries after the fabrication process, leaving behind a highly mesoporous structure with a complex bulk geometry. These mesoporous structures are well-suited for diverse sensing applications [3, 6, 7].

Electrically conductive particles can be dispersed into hydrogels to achieve electrical conduction. Electrically conductive hydrogels can be used for various sensing applications such as humidity sensing and touch sensing [8]. Virtuous to their electrical conductivity, these hydrogels can also be used as heaters [6].

The recent emergence of the COVID-19 pandemic has highlighted the necessity for the development of sensors capable of detecting human interactions with their environment. This is essential due to the virus' potential to be transmitted through direct human-to-human contact or indirectly via contaminated surfaces. Research has shown that the virus can remain viable for up to 5 days on surfaces made of polymeric, metallic, and ceramic materials [9]. Furthermore, it is a common human tendency to frequently touch their mouth, nose, and eyes involuntarily, which significantly increases the risk of viral transmission to and from common-use objects [10]. Consequently, it is essential to identify instances of human-to-surface contact on common-use objects and subsequently employ effective virucidal methods for disinfection. These virucidal techniques include the use of soapy water, exposure to virucidal chemicals, exposure to ultraviolet radiation, and the application of heat [11, 12].

A pre-symptomatic carrier might enter the workplace undetected, which may lead to the exposure of the workforce to the virus. Furthermore, the use of common equipment such as toolboxes, equipment closets, and control panels may lead to indirect transmission of the virus. The manual disinfection of common-use equipment after every user interaction cannot be guaranteed due to their frequency of use.

Various touch detection sensors are reported in the literature such as photoelectric, ultrasonic, and capacitive sensors. The capacitive sensing technique is widely implemented for touch sensing in various applications such as keypads for appliances and smartphones and can be employed for touch detection on target surfaces [13, 14].

Various active disinfection systems have been reported in the literature for SARS-CoV-2. Murthy proposed a system for disinfecting luggage using ultraviolet light [15]. Mahida et al. developed Tru-D™, an ultraviolet-based active

disinfection device targeted for killing microorganisms in a confined space [16]. Yang et al. conducted an experimental study to validate the effectiveness of an ultraviolet-based Hyper Light Disinfection robot in eradicating different types of pathogens [17]. UV-irradiation has proven to be an effective virucide and can be employed to disinfect the equipment stored in closets. However, the hazardous nature of UV radiation limits its use in the disinfection of equipment during a work shift in the presence of personnel.

Thermal disinfection using heated chambers has also been implemented for decades; however, it has not received much attention in active disinfection systems targeted for SARS-CoV-2. An example of thermal disinfection of N95 facemasks has been reported [18]. Thermal disinfection works by the destruction of the protein capsid of the virus that protects its genetic material. Lentivirus is an RNA virus with a protein capsid similar to SARS-CoV-2 that is commonly used to imitate viral growth in lab environments. The virus can be used to determine the thermal destruction temperature of the protein capsid.

The common-use equipment can be retrofitted with 3D-printed disinfection heaters; however, the equipment cannot be constantly kept at high temperatures since above 55 °C is hazardous for humans to touch [19]. Therefore, a smart disinfection system is necessary to detect human interactions with common-use equipment and then take disinfection measures. The equipment will be safe for human interaction once its temperature drops below 55 °C. The handles of the common-use equipment are the potentially contaminated surfaces that humans may interact with repeatedly. Therefore, automatic disinfection systems can be applied to the common-use equipment handles to attenuate the virus spread.

3D-printed heating elements made from electrically conductive hydrogels can serve the dual purpose of capacitive sensing electrodes. However, the electrically conductive hydrogel composites found in the literature have electrical conductivities in the range of 10^{-4} to 10^1 S.m⁻¹ [20, 21]. Therefore, these hydrogels cannot be employed to manufacture heaters due to their limited current carrying capacity. Furthermore, the hydrogel must be able to sustain temperatures as high as the operating temperature of the heater. Nevertheless, the rheology of the hydrogel must be suitable for the 3D-printing process. Therefore, a 3D-printable, thermally stable, and electrically conductive hydrogel composite must be developed for the application of 3D-printed heating systems.

In this article, we propose a novel electrically conductive hydrogel composite and present its application in the development of a novel smart touch detection and disinfection system that employs an additively manufactured heating element made from an electrically conductive hydrogel that can function dually as a capacitive sensor. The thermal

destruction temperature and exposure time for the protein capsid of viruses were optimized and adopted for disinfection. The article reports the development of the system and its characterization along with its application on the door handles.

2 Development of electrically conductive composite hydrogel

2.1 Synthesis of electrically conductive composite hydrogel

The hydrogel matrix was synthesized by dissolving sodium carboxymethyl cellulose 5% w/w in DI water. The solution was stirred mechanically until the hydrogel was homogenized. Next, graphite microparticles were added as reinforcement to the hydrogel to produce an electrically conductive composite hydrogel. Three distinct compositions 1:9 (1G9), 2:8 (2G8), and 3:7 (3G7), were produced based on the ratio of the graphite particles to the hydrogel w/w.

2.2 Material characterization

The developed electrically conductive composite hydrogels were characterized for their morphology, electrical conductivity, and thermal degradation.

2.2.1 Morphology

The morphology of the electrically conductive composite hydrogel was studied under a scanning electron microscope. The SEM micrographs show that the reinforcing graphite particles have percolated and formed a porous structure which is held together by the polymeric strands of the hydrogel. The graphite particles form a path for the flow of electrons, and therefore, electrical conductivity is achieved in the host hydrogel. The SEM micrographs are presented in Fig. 1.

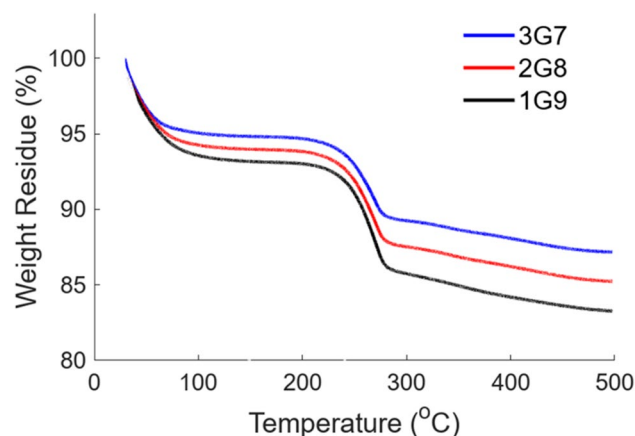


Fig. 2 Thermal degradation of electrically conductive composite hydrogels 1G9, 2G8, and 3G7

2.2.2 Thermal degradation

The thermal degradation of the electrically conductive composite hydrogel was studied using thermogravimetric analysis under the heating regime of 5 °C/min in a dry air environment. The thermal degradation of the composite hydrogels is presented in Fig. 2.

The loss in mass below 100 °C is attributed to the evaporation of moisture in the samples. There is no degradation of the composite hydrogels between 100 and 200 °C; however, the samples rapidly degrade between 225 and 275 °C. Therefore, it can be concluded that the developed composite hydrogel is safe to use in applications up to 200 °C.

2.2.3 Rheology

The rheology of hydrogel plays an important role in its 3D printability. The hydrogel must not only be able to flow through the fine nozzle of the 3D-printing tool head but also have enough yield strength to bear the load of the

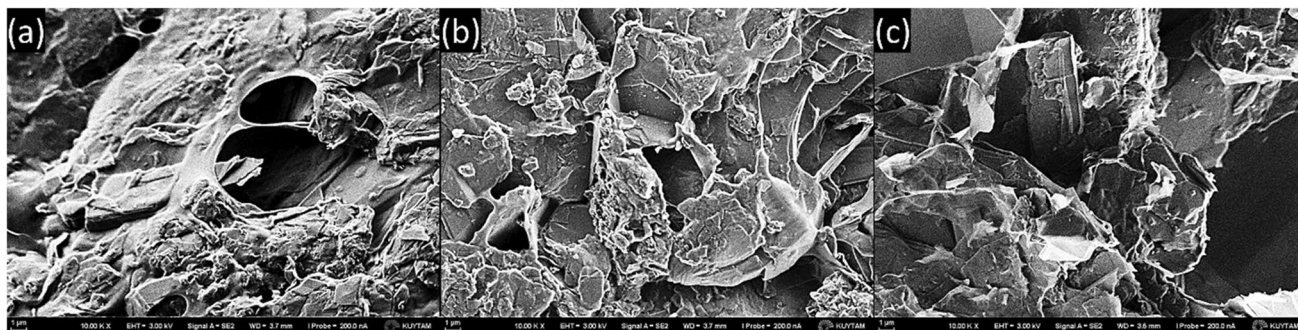


Fig. 1 SEM micrographs of electrically conductive composite hydrogels. a 1G9, b 2G8, and c 3G7

subsequent hydrogel layers. Rheology is characterized by Herschel–Berkley’s model for non-Newtonian fluids presented in Eq. 1.

$$\tau = \tau_0 + K\dot{\gamma}^n \quad (1)$$

where τ is the shear strength, τ_0 is the yield strength, K is the consistency factor, $\dot{\gamma}$ is the shear rate, and n is the dimensionless flow index of the hydrogel.

The rheology of the developed hydrogel composites was analyzed on the Malvern Kinexus pro rheometer using the flat plate test geometry and the gap of 3 mm. The viscosity and the shear stress versus the shear rate are presented in Fig. 3.

The Herschel–Berkley parameters for the developed hydrogel composites are tabulated in Table 1. The hydrogel composites behave like a typical non-Newtonian fluid having a high viscosity at rest whereas the viscosity drops as

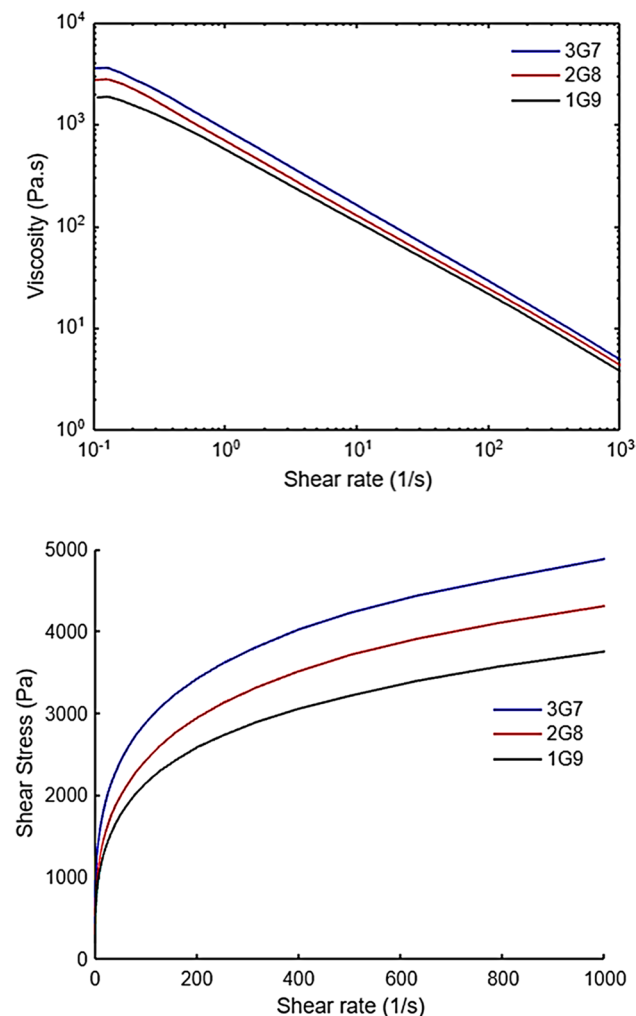


Fig. 3 Viscosity and Shear stress versus the shear rate of electrically conductive composite hydrogels 1G9, 2G8, and 3G7

Table 1 Herschel–Berkley parameters for the developed hydrogel

Hydrogel	τ_0 (Pa)	K (Pa.s ⁿ)	n
1G9	191	590	0.27
2G8	273	690	0.6
3G7	350	900	0.24

the shear is applied. This reduction in the viscosity enables the hydrogel to flow through the nozzle of the 3D printing tool head. The viscosity rises back to the rest viscosity when the hydrogel has been deposited. The yield strength of the hydrogel enables it to bear the load of the subsequent layers. The rheological properties match well with the recommended rheology for 3D printing in the literature [22].

2.2.4 Electrical conductivity

The electrical conductivity of the composite hydrogel was characterized by the 2-probe method. The resistances of the samples were recorded by a digital multimeter and the resulting electrical conductivity (k) was calculated by using Eq. 2.

$$k = \frac{l}{RA} \quad (2)$$

The electrical conductivity of the composite hydrogel increases with the increasing graphite loading. The maximum electrical conductivity achieved is ~ 145 (S.m⁻¹). The electrical conductivity of all three composite hydrogels is presented in Table 2.

The electrical conductivity achieved by the composite hydrogel shall enable its application as a capacitive touch sensor for the detection of human interactions. Furthermore, the composite hydrogel can also be used to develop disinfection heaters.

3 Determination of the disinfection temperature

The temperature-based insulation on a lentivirus system with a protein capsid similar to SARS-CoV-2 is tested experimentally to determine the thermal disinfection temperature.

Table 2 Electrical conductivities of electrically conductive composite hydrogels 1G9, 2G8, and 3G7

Composite hydrogel	Electrical conductivity (S.m ⁻¹)
1G9	113.4 ± 3.2
2G8	127.7 ± 2.4
3G7	145.3 ± 2.2

Green fluorescent protein (GFP) lentiviruses were synthesized to visualize virus infection.

3.1 Virus production

HEK293T cells with low passage number (< 10–15) were seeded into a 10-cm plate to have a 70–80% confluent plate the next day (in D-10 medium, incubated overnight at 37–5% CO₂ incubator). Ten micrograms of the GFP plasmid and pLenti CMV virus plasmids (9 µg pCMV-dR8.2 dvpr and 1 µg pCMV-VSVG) were mixed with transfection reagent (PEI) and incubated at room temperature for 10 min. A 5-ml medium of HEK293T cells was discarded, and the transfection mix was added to the cells drop-wise, swirled, and incubated overnight. On day 3, 3 ml fresh D10 medium was added to each plate without disturbing the transfected cells and incubated overnight. On day 4 (48 h after transfection) medium was replaced with 8-ml fresh D10 medium, and the plate was incubated for 24 h. On day 5 (72 h after transfection), 8-ml medium containing lentiviral particles were harvested into 50-ml falcon and stored at 4 °C (till the next harvesting), and 8-ml fresh D10 medium was added to the plate and incubated for 24 h. On day 6, an 8-ml medium containing lentiviral particles was harvested into the previously harvested 8-ml medium. All the harvested media (total 16 ml) was filtered using a 0.45-µm filter. Lentiviral particles were stored at –80 °C until the viral infection procedure was conducted.

$$\text{Transfection efficiency in \%} = 100 \times (\# \text{ of cells with GFP signal} / \# \text{ of total cells}) \quad (3)$$

The viruses were exposed to heat for different durations (1–5 min) and at various degrees (60, 65, 75 °C) to determine the effect of heat on viral integrity. As a positive control of microscope images, some U2OS cells were transduced with a set of viruses that were not exposed to heat, and as a negative control, some U2OS cells were not transduced with viruses at all. The efficiency of virus infectivity differed depending on the duration and degree of the temperature applied to viruses. The microscope images in Fig. 4 show that virus infectivity decreases as the temperature and exposure time increase. The viral viability dropped nearly to zero with heat application of 5 min at 60 °C, 5 min at 65 °C, and 3 min at 75 °C. The number of cells with a GFP signal was normalized according to the positive control and evaluated as 100% in fluorescent microscope images. The percentage of virus viability versus different exposure temperatures and times is presented in Fig. 5.

It can be concluded that viruses can be inactivated after 5 min of exposure at 60 °C and 65 °C. However, the disinfection time can be reduced to 3 min by increasing the

3.2 Viral Infection

U2OS cells (passage numbers 12–15) were seeded into three six-well plates to have a 70–80% confluent plate the next day. On day 2, virus-containing solutions were incubated at 60, 65, or 75 °C for 1, 2, 3, 4, or 5 min and then mixed with the mixture of 250 µl DMEM and 1 µl protamine sulfate (8 µg/µl). After removing the media from the cells, this mixture was added to U2OS cells. As a positive control of the virus infection, the virus-containing solution was incubated at room temperature and then mixed with the mixture of 250 µl DMEM and 1 µl protamine sulfate (8 µg/µl). As a negative control, the previous media was replaced only with 1 ml of DMEM. The cells were incubated at 37 °C, 5% CO₂ overnight. On day 3, viral media was removed, and 1.5 ml fresh medium was added to each well.

3.3 Determination of thermal disinfection temperature

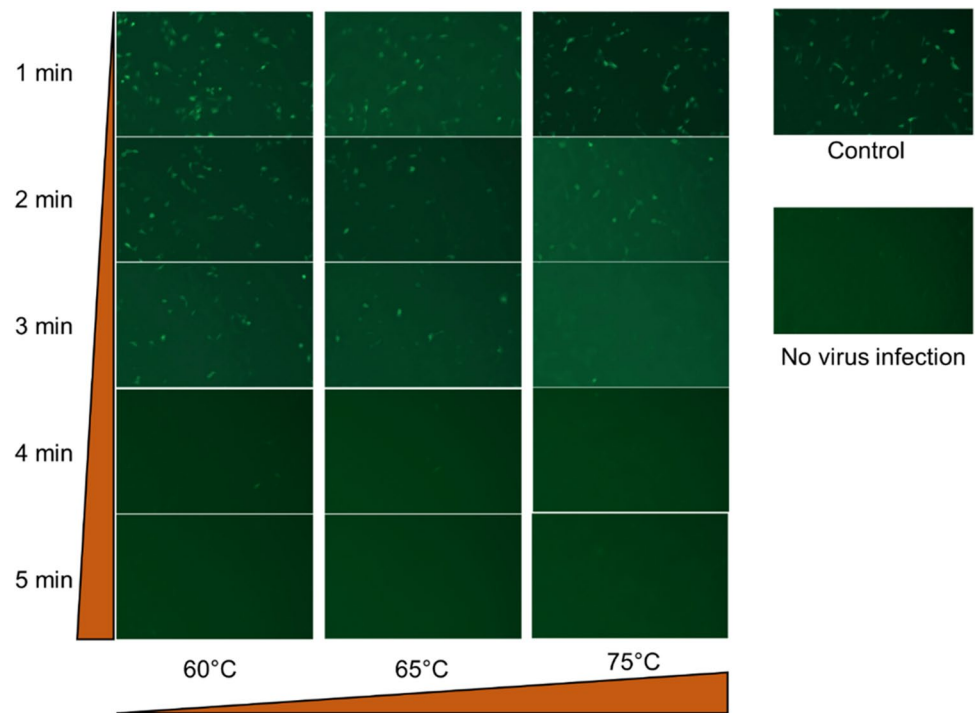
Twenty-four hours after the viral infection, the media was removed from the plates, and each well was analyzed using a fluorescent microscope under a widefield and EGFP filter. The fluorescent micrographs illustrating the effect of temperature and time on the infectivity of the virus are presented in Fig. 4. The number of cells under widefield and EGFP filter was counted, and the transfection efficiency was calculated according to Eq. 3.

temperature to 75 °C. Therefore, an automatic disinfection system may be developed as a countermeasure to the spread of viruses; the system will heat a potentially contaminated surface to 60–75 °C after it has been touched by a user.

4 Development of an automatic touch detection and disinfection system

The automatic touch detection and disinfection system are implemented on a closet door handle that comprises an additively manufactured electrode that operates in dual mode. In touch detection mode, the electrode is used to detect the touch of a human body on its surface, whereas, in the disinfection mode, the same electrode is used as a heating system. The switching between the touch detection mode and the disinfection mode is achieved through a control circuit. Visual feedback is provided through an LCD that indicates the unsafe/safe-to-touch status of the door handle.

Fig. 4 Fluorescent microscope visuals illustrating the effect of temperature and time on the infectivity of the virus



4.1 Additive manufacturing of the door handle

The fused filament fabrication (FFF) technique and the direct ink writing (DIW) technique were used to develop a multi-material additive manufacturing setup. The FFF and the DIW heads were mounted together on the end effector of the Mitsubishi Electric robotic manipulator. The FFF head enables the deposition of polylactic acid (PLA) using a 0.3-mm nozzle,

while the DIW head enables the deposition of electrically conductive composite hydrogel using a 0.4-mm nozzle. The 3G7 hydrogel was employed as it yielded the best electrical conductivity. The combination of the FFF and DIW heads enables the selective deposition of electrically conducting and insulating regions in a single build. Figure 6a illustrates the multi-material additive manufacturing setup. The process parameters used for additive manufacturing are presented in Table 3.

Fig. 5 The bar graph illustrating the percentage of virus viability versus different exposure temperatures and times

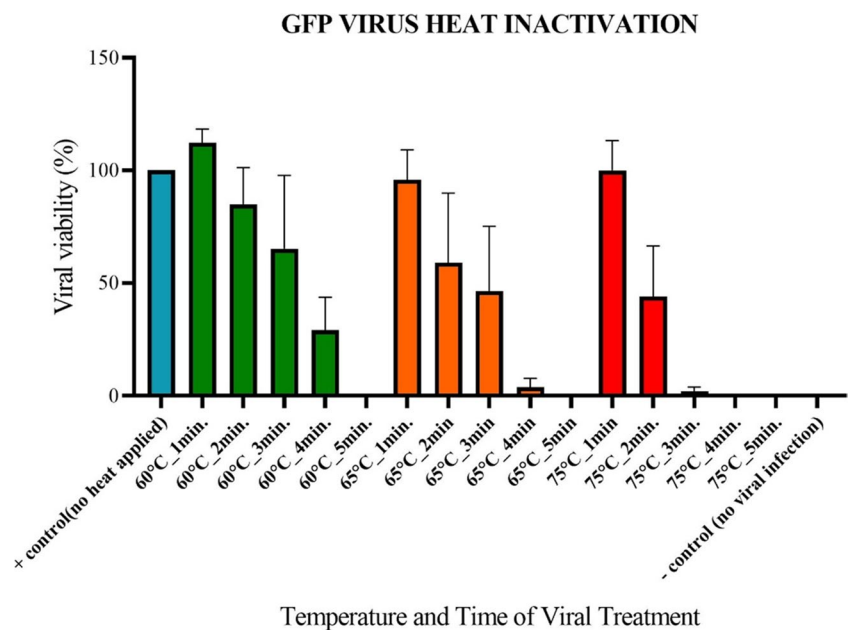


Table 3 Parameters of the multi-material additive manufacturing process

	Parameter	Value
FFF	Nozzle diameter	0.3 mm
	Layer height	0.2 mm
	Extrusion width	0.3 mm
	Linear speed	50 mm.s ⁻¹
	Raster angle	45°
	Infill pattern	Rectilinear
	Infill density	25%
	Number of shells	2
	Material	PLA
	Nozzle temperature	200 °C
DIW	Nozzle diameter	0.4 mm
	Layer height	0.2 mm
	Extrusion width	0.6 mm
	Linear speed	20 mm.s ⁻¹
	Raster angle	45°
	Infill pattern	Rectilinear
	Infill density	100%
	Number of shells	2
Material	Hydrogel (3G7)	
Air pressure	0.2 MPa	

The door handle is additively manufactured using a multi-material robotic additive manufacturing setup. The door handle is designed to be mounted using two additively manufactured mounting brackets. The door handle dimensions are kept in line with the anthropometric data for an adult hand with a grip length of 100 mm and a cross-section of 40 mm × 30 mm [23]. The chassis and the mounting brackets of the door handle are manufactured from polylactic acid (PLA) using the FFF head, while the embedded capacitive sensing electrode/disinfection heater is manufactured from an electrically conductive polymer composite using the DIW head. The door handle was coated with graphite-loaded epoxy to ensure waterproofing before mounting it on the closet door. The CAD model of the door handle along with the rectilinear deposition pattern of the hydrogel is illustrated in Fig. 6b, and the automatic disinfection system mounted on a closet door is shown in Fig. 6c.

4.2 Touch detection mode

The touch detection system employed in this paper is based on the principle of capacitive sensing. The capacitive sensor is configured in a self-capacitance mode, where an additively manufactured electrode is subjected to an alternating voltage source. The electric charge is stored on the surface of an electrode in the form of an electric field and is known as the self-capacitance of the electrode. Owing to the conductive nature of the human body and

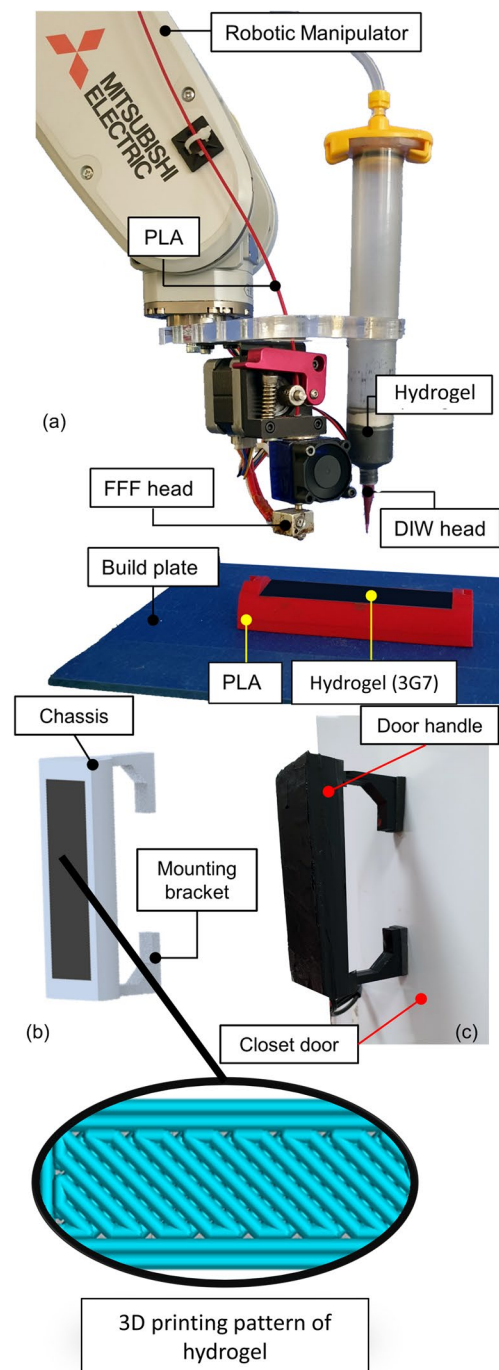


Fig. 6 **a** The multi-material robotic 3D-printing setup, **b** the CAD model of the door handle along with the rectilinear deposition pattern of the hydrogel, and **c** the automatic disinfection system mounted on a closet door

dielectric properties, when the human body interacts with the electrode's electric field, the overall density of the stored electric charge varies. The variation in the charge density with respect to the interacting external body brings a shift in the self-capacitance of the electrode. This change in self-capacitance is used for touch detection. The

electrode is attached in parallel with an inductor-capacitor (LC) resonating circuit driven by a commercially available frequency-to-digital converter (FDC). The LC resonator oscillates at a frequency of 40 MHz. The change in the self-capacitance of the electrode, consequent to the interacting human body, varies the frequency of the LC resonator. Figure 7 illustrates the schematics of the self-capacitance-based touch detection system.

The LC resonator is comprised of an inductor $L_1 = 10\mu\text{H}$ and a capacitor $C_1 = 39\text{pF}$, the variable capacitor C_v indicates a sum of the self-capacitance C_t between the electrode and the interacting human body, the parasitic capacitance C_p of the circuit, the capacitance C_e between the electrode and the ground and the capacitance C_c between the electrode and the electrical connections. The variation in the capacitances C_p, C_e , and C_c are negligible as compared to the self-capacitance C_t therefore they are assumed to be constant throughout the experiment. The self-capacitance C_t depends on various human factors such as the size, thickness, and number of fingers in contact with the sensor.

The change in the self-capacitance of the electrode, consequent to the interacting human body, varies the frequency of the LC resonator. This change in the frequency is measured by the FDC and is converted into equivalent capacitance using Eq. 4.

$$F = \frac{1}{2\pi\sqrt{L_1 C}} \quad (4)$$

where C is the equivalent capacitance of the whole system and is denoted by a summation of C_1 and C_v , as illustrated in Eq. 5.

$$C = C_1 + C_v \quad (5)$$

The resonance frequency of the system decreases when it comes in contact with the human hand. Removing the human hand from the capacitive circuit increases the resonance frequency.

4.3 Disinfection mode

Electrical current is passed through the additively manufactured heating element in the disinfection mode. The

temperature of the heating element is controlled by a proportional integral derivative (PID) controller that employs an NTC 100 k thermistor for feedback. The heat (Q) generated by the heating element is represented by Joule's equation presented in Eq. 6.

$$Q = VI t \quad (6)$$

where V is the voltage applied to the heating element, I is the current drawn by the heating element, and t is the heating duration. The voltage applied to the disinfection heater is controlled by the PID controller, and the current drawn is recorded by an ACS712 current sensor. The maximum power consumed by the heater is 25 W. The heater was characterized by its heating and cooling responses for the target temperatures of 70 °C, 75 °C, and 80 °C. The heater is passively cooled by the ambient air. The heating and cooling responses of the system were utilized to tune the proportional, integral, and derivative gains of the PID controller.

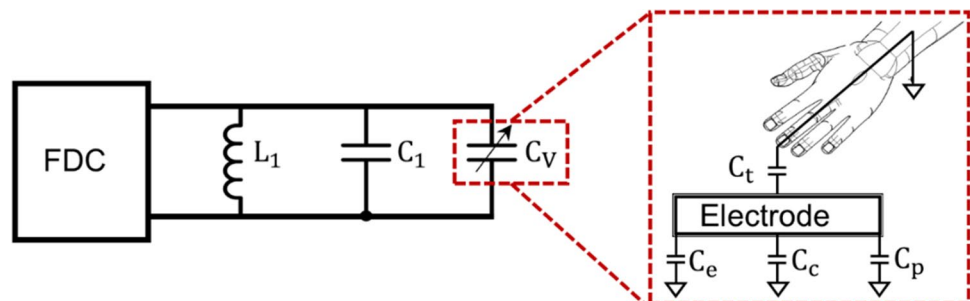
4.4 Disinfection on-demand algorithm

An 8-bit microcontroller is used to integrate the touch detection mode, disinfection mode, and LCD status indicator. The system starts in the touch detection mode and waits for human interaction while the LCD indicates the "Safe to touch" status. The disinfection module is triggered after the end of a human interaction detected by the touch detection module. The system is heated to the disinfection temperature followed by an isothermal hold. The LCD indicates the "Do not touch" status during the disinfection mode. The end of the disinfection mode reverts the system to touch detection mode, while the LCD indicates a "Do not touch" status till the temperature of the system drops below 55 °C, which makes the system safe to touch, and the LCD shows the same. The flowchart of the disinfection on-demand algorithm is illustrated in Fig. 8.

4.5 Characterization of the touch detection sensor

The response of the capacitive sensing module to human touch is illustrated in Fig. 9. The door handle is in contact with the surrounding air initially, and there is no significant

Fig. 7 The schematic of the self-capacitance-based touch detection system



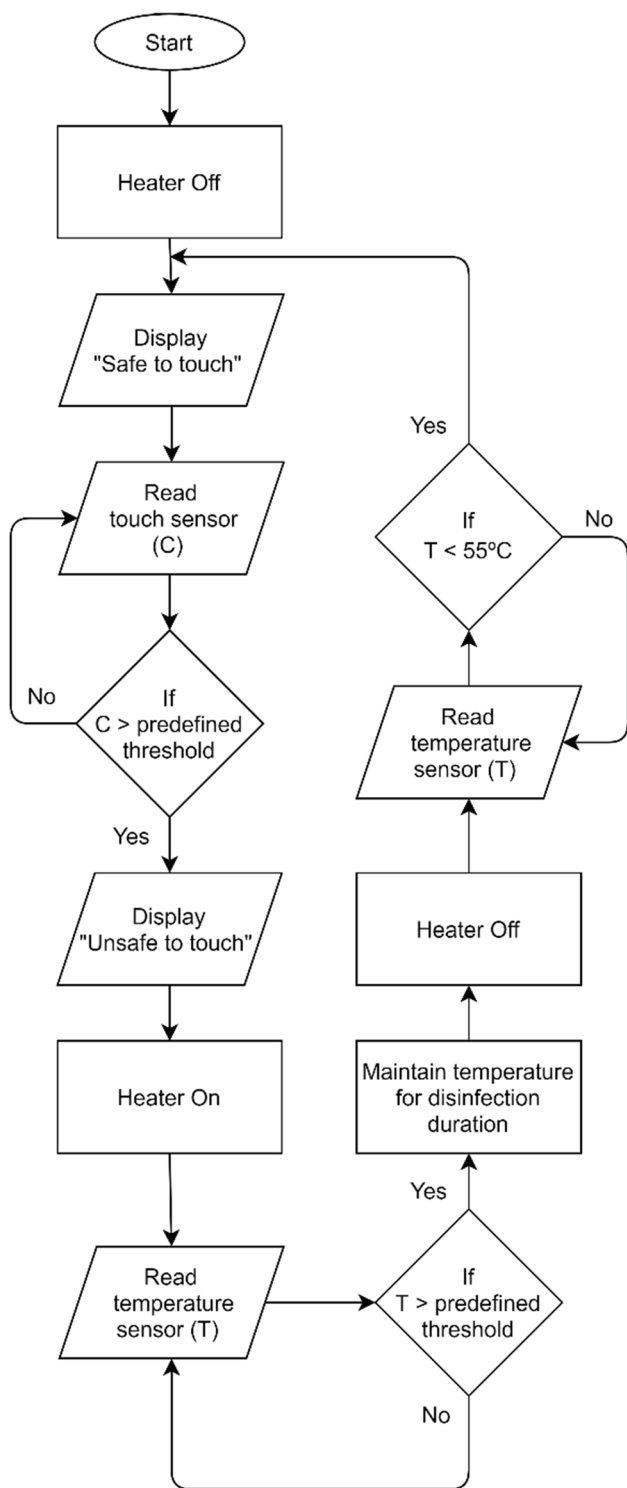


Fig. 8 Flowchart of the disinfection on-demand algorithm

change in the resonance frequency of the LC circuit. The human interaction with the surface of the door handle causes a sharp decrease in the resonance frequency due to the higher dielectric of the human hand compared to that of air. This sharp decrease is reflected by the negative peak

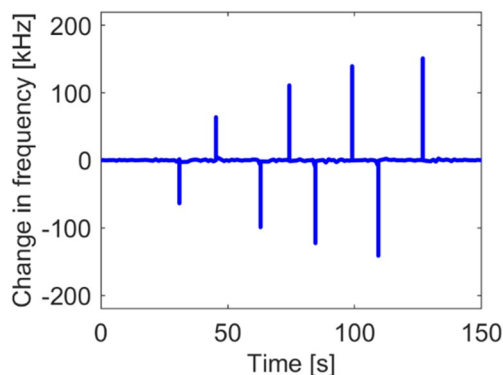


Fig. 9 The response of the capacitive touch detection sensor for pinch grip (first pair of peaks), 2-finger claw grip (second pair of peaks), 3-finger claw grip (third pair of peaks), and 4-finger claw grip (fourth pair of peaks)

in the change in frequency trend. The shift in frequency remains insignificant during the engagement. The resonance frequency increases when the human hand disengages the door handle, which is recorded as an indication of the end of human interaction. The subsequent peaks reflect the variations in the magnitude of the resonance frequency due to the difference in the grip type. The variations in the magnitude of change in frequency for various test subjects and grip styles are tabulated in Table 4. A ± 40 kHz change in the frequency is adopted as the threshold for detecting a touch.

4.6 Characterization of disinfection heater

The response of the disinfection heater for the disinfection temperatures of 60 °C, 65 °C, and 75 °C is illustrated in Fig. 10. The rise time, hold time, and cooldown time to 55 °C of the disinfection strategies are tabulated in Table 5. The results indicate that the 60 °C strategy yields the lowest cycle time out of the three routines. Therefore, 60 °C is selected for the automatic disinfection system.

4.7 Disinfection on-demand

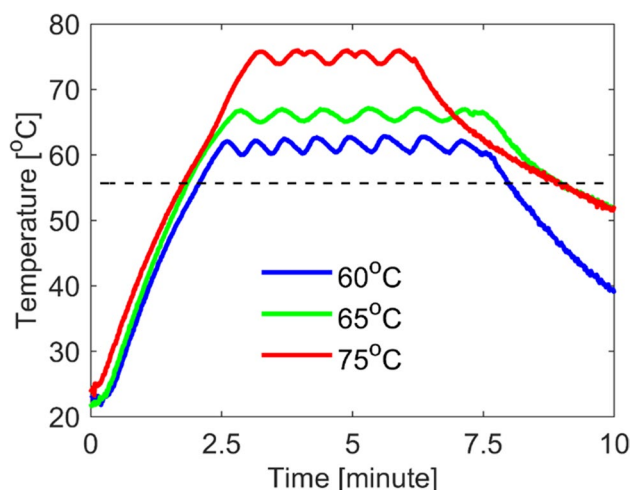
The integration of the sensing and disinfection module for the 60 °C disinfection strategy is illustrated in Fig. 11. The system remains safe to touch (high) and becomes unsafe to touch (low) when the touch detection sensor detects human interaction. The controller detects the end of human interaction and performs the prescribed heating for disinfection. The system becomes safe to touch and waits for the next user interaction after its temperature drops below 55 °C.

4.8 Efficacy of the system

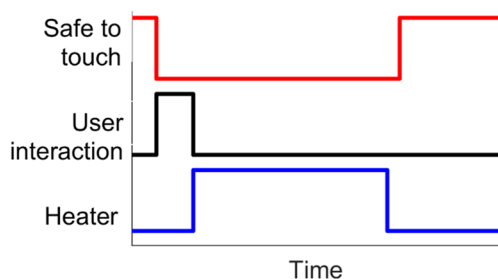
The ability to trigger disinfection measures based on the detection of human interactions enables the automatic

Table 4 The changes in the resonance frequency for various test subjects

Test subject	Change in frequency (kHz)			
	Pinch grip	2-finger claw grip	3-finger claw grip	4-finger claw grip
1	±96	±140	±174	±198
2	±62	±100	±118	±126
3	±64	±98	±122	±151

**Fig. 10** The evolution of the temperature of the door handle for 60 °C, 65 °C, and 75 °C disinfection strategies and their respective exposure times**Table 5** The rise, hold, cooldown, and total cycle time of the 60 °C, 65 °C, and 75 °C disinfection strategies along with their respective energy consumption

Disinfection temperature (°C)	Rise time (minute)	Hold time (minute)	Cooldown to 55 °C time (minute)	Total cycle time (minute)	Energy consumption (Wh)
60	2.6	5	0.3	7.9	1.64
65	2.8	5	1.2	9	1.73
75	3.2	3	2.8	9	1.69

**Fig. 11** The digital response of the touch detection system for the 60 °C disinfection strategy

disinfection system to attenuate the indirect spread of SARS-CoV-2. The automatic disinfection system automatically disinfected the door handles at the cost of roughly 1.64 Wh of energy to prepare the equipment for the next user interaction. Automated disinfection significantly reduces the load on the janitorial staff and does not need human evacuation from the system. The total cycle time of the system is approximately 8 min and is suited for applications where the expected number of interactions in an 8-h work shift is less than 60. The additive manufacturability of the system enables the flexibility in design needed for the adaptation of the system in various industrial applications such as the handles of power tools, closet doors, refrigerator doors, and the door of control panels.

5 Conclusion

In summary, the article presents the development and characterization of a 3D-printable and electrically conductive composite hydrogel and its application for creating a smart disinfection system for common-use equipment and surfaces. The developed hydrogel yields an electrical conductivity of $145 \text{ S}\cdot\text{m}^{-1}$, is thermally stable up to 200 °C and has a 3D printable rheology. The developed composite was employed to create a smart disinfection system. The system detects human interactions and takes disinfection measures using a low-powered and additively manufactured disinfection heater that serves the dual purpose of a capacitive touch sensor providing feedback of human interaction. The thermal disinfection temperature and exposure time for viruses with a protein capsid similar to SARS-CoV-2 were investigated and employed as operating parameters of the system. The response of the capacitive sensor was characterized for various types of grips, and different disinfection strategies were tested. The disinfection strategy of 60 °C with a 5-min exposure time was selected owing to its lower energy consumption of 1.64 Wh. The system becomes safe to touch when its temperature drops below 55 °C, and an LCD indicates the same. The additive manufacturability of the system renders the system adaptable in various industrial applications where the expected user interactions are less than or equal to 60 interactions in an 8-h work shift.

Acknowledgements This research was supported by the Manufacturing and Automation Research Center, Koc University Istanbul, Turkey. The authors acknowledge Mitsubishi Electric for providing the robotic manipulator used in the multi-material additive manufacturing setup.

Author contribution SAK: conceptualization, investigation, methodology, and writing—original draft.

ANM: conceptualization, investigation, methodology, writing—original draft.

BV: conceptualization, investigation, methodology, writing—original draft.

SG: conceptualization, methodology, writing—original draft.

IHK: supervision, project administration, conceptualization, methodology, writing—review and editing.

IL: supervision, funding acquisition, project administration, conceptualization, investigation, methodology, writing—original draft, writing—review and editing.

Data availability The data are available from the corresponding author on request.

Declarations

Conflict of interest The authors declare no competing interests.

Open Access This article is licensed under a Creative Commons Attribution 4.0 International License, which permits use, sharing, adaptation, distribution and reproduction in any medium or format, as long as you give appropriate credit to the original author(s) and the source, provide a link to the Creative Commons licence, and indicate if changes were made. The images or other third party material in this article are included in the article's Creative Commons licence, unless indicated otherwise in a credit line to the material. If material is not included in the article's Creative Commons licence and your intended use is not permitted by statutory regulation or exceeds the permitted use, you will need to obtain permission directly from the copyright holder. To view a copy of this licence, visit <http://creativecommons.org/licenses/by/4.0/>.

References

1. M. Sobczyk, S. Wiesenhütter, J.R. Noennig, T. Wallmersperger, Smart materials in architecture for actuator and sensor applications: a review. *J. Intell. Mater. Syst. Struct.* **33**(3), 379–399 (2022). https://doi.org/10.1177/1045389X211027954/ASSET/IMAGES/LARGE/10.1177_1045389X211027954-FIG11.JPEG
2. D. Yan, Z. Wang, Z. Zhang, Stimuli-responsive crystalline smart materials: from rational design and fabrication to applications. *Acc. Chem. Res.* **55**(7), 1047–1058 (2022). https://doi.org/10.1021/ACS.ACCOUNTS.2C00027/ASSET/IMAGES/LARGE/AR2C00027_0009.JPEG
3. S.S. Ashok Sharma, S. Bashir, R. Kasi, R.T. Subramaniam, The significance of graphene based composite hydrogels as smart materials: a review on the fabrication, properties, and its applications. *FlatChem* **33**, 100352 (2022). <https://doi.org/10.1016/J.FLATC.2022.100352>
4. Adebayo, A. O., Alli, Y. A., Bamisaye, A., & Adewuyi, S. (2023). Nano chitosan anchored copper-ferrite: a smart magnetic nanocomposite agent for drug delivery. *Emergent. Mater.* 1–9. <https://doi.org/10.1007/S42247-023-00584-Y/FIGURES/5>
5. Glingasorn, B., Yongsapanan, N., Pangon, A., Lin, C., & Ummartyotin, S. (2023). Synthesis of bioinspired based hydrogel composite from hyaluronic acid/polyacrylic acid and lignin as an adhesive for medical technology. *Emergent. Mater.* 1–10. <https://doi.org/10.1007/S42247-023-00592-Y/FIGURES/8>
6. S.A. Khan, I. Lazoglu, Development of additively manufacturable and electrically conductive graphite–polymer composites. *Progress in Additive Manufacturing* **5**(2), 153–162 (2020). <https://doi.org/10.1007/S40964-019-00102-9/FIGURES/14>
7. C. Maity, N. Das, 2021 Alginate-based smart materials and their application: recent advances and perspectives. *Topics. Curr. Chem.* **380**(1), 1–67 (2021). <https://doi.org/10.1007/S41061-021-00360-8>
8. P. Parthasarathy, Graphene/polypyrrole/carbon black nanocomposite material ink-based screen-printed low-cost, flexible humidity sensor. *Emergent. Mater.* **6**(6), 2053–2060 (2023). <https://doi.org/10.1007/S42247-023-00585-X/FIGURES/11>
9. G Kampf, D Todt, S Pfaender, & E Steinmann (2020). Persistence of coronaviruses on inanimate surfaces and their inactivation with biocidal agents. In *Journal of Hospital Infection* (Vol. 104, Issue 3, pp. 246–251). W.B. Saunders Ltd. <https://doi.org/10.1016/j.jhin.2020.01.022>
10. A.M. Wilson, M.P. Verhougstraete, P.I. Beamer, M.F. King, K.A. Reynolds, C.P. Gerba, Frequency of hand-to-head, -mouth, -eyes, and -nose contacts for adults and children during eating and non-eating macro-activities. *J. Eposure Sci. Environ. Epidemiol.* **31**(1), 34–44 (2021). <https://doi.org/10.1038/s41370-020-0249-8>
11. M.M. Mahat, A.S.M. Sabere, J. Azizi, N.A.N. Amdan, Potential applications of conducting polymers to reduce secondary bacterial infections among COVID-19 patients: a review. *Emergent Materials* **4**(1), 279–292 (2021). <https://doi.org/10.1007/S42247-021-00188-4>
12. M. Jariyaboon, P. Masrinoul, J. Komaikul, K. Muenkaew, S. Juntarapornchai, K. Ketsuwan, E. Rodpai, S. Ruangdachsuwan, S. Palabodeewat, C. Chitichotpanya, Optimization of Ag-TiO₂ nanocomposite at a low toxicity dose as a self-virucidal disinfectant against COVID-19. *Emergent. Mater.* **6**(4), 1259–1272 (2023). <https://doi.org/10.1007/S42247-023-00520-0/FIGURES/12>
13. A.H. Anwer, N. Khan, M.Z. Ansari, S.S. Baek, H. Yi, S. Kim, S.M. Noh, C. Jeong, Recent advances in touch sensors for flexible wearable devices. *Sensors* **22**(12), 4460 (2022). <https://doi.org/10.3390/S22124460>
14. Y. Lee, J. Kim, B. Jang, S. Kim, B.K. Sharma, J.H. Kim, J.H. Ahn, Graphene-based stretchable/wearable self-powered touch sensor. *Nano Energy* **62**, 259–267 (2019). <https://doi.org/10.1016/J.NANOEN.2019.05.039>
15. G.S. Murthy, An automatic disinfection system for passenger luggage at airports and train/bus stations. *Trans Indian Natl Acad Eng* **5**(2), 295–298 (2020). <https://doi.org/10.1007/s41403-020-00131-9>
16. N. Mahida, N. Vaughan, T. Boswell, First UK evaluation of an automated ultraviolet-C room decontamination device (Tru-D™). *J. Hosp. Infect.* **84**(4), 332–335 (2013). <https://doi.org/10.1016/j.jhin.2013.05.005>
17. J.H. Yang, U.I. Wu, H.M. Tai, W.H. Sheng, Effectiveness of an ultraviolet-C disinfection system for reduction of healthcare-associated pathogens. *J. Microbiol. Immunol. Infect.* **52**(3), 487–493 (2019). <https://doi.org/10.1016/j.jmii.2017.08.017>
18. GH Borschel, SC Daeschler, N Manson, K Joachim, A W H Chin, K Chan, PZ Chen, K Tajdaran, K Mirmoeini, JJ Zhang, JT Maynes, M Science, A Darbandi, D Stephens, LLM Poon, & F Gu (2020) Reprocessing N95 respirators during the COVID-19 pandemic: moist heat inactivates SARS-CoV-2 and maintains N95 filtration. In *medRxiv* (p. 2020.05.25.20112615). medRxiv. <https://doi.org/10.1101/2020.05.25.20112615>
19. BS EN 13202:2000. (2000). *Ergonomics of the thermal environment - temperatures of touchable hot surfaces - guidance for establishing surface temperature limit values in production standards with the aid of EN 563*
20. G. Kougkolos, M. Golzio, L. Laudebat, Z. Valdez-Nava, E. Flahaut, Hydrogels with electrically conductive nanomaterials for

- biomedical applications. *J. Mater. Chem. B* **11**(10), 2036–2062 (2023). <https://doi.org/10.1039/D2TB02019J>
21. B. Khan, S. Abdullah, S. Khan, Current progress in conductive hydrogels and their applications in wearable bioelectronics and therapeutics. *Micromachines* **14**(5), 1005 (2023). <https://doi.org/10.3390/M14051005>
 22. S. Tagliaferri, A. Panagiotopoulos, C. Mattevi, Direct ink writing of energy materials. *Mater. Adv.* **2**(2), 540–563 (2021). <https://doi.org/10.1039/D0MA00753F>
 23. Wang, C. Y., & Cai, D. C. (2017). Hand tool handle design based on hand measurements. *MATEC Web of Conferences*, 119. <https://doi.org/10.1051/mateconf/201711901044>